Deposition reactors for solar grade silicon: a comparative thermal analysis of a Siemens reactor and a fluidized bed reactor

A. Ramos[a,1,*], W. O. Filtvedt[b], D. Lindholm[b], P. A. Ramachandran[c], A. Rodríguez[d], and C. del Cañizo[a]

[a]Instituto de Energía Solar - Universidad Politécnica de Madrid, ETSI Telecomunicación, 28040 Madrid, Spain
[b]Institute for Energy Technology -IFE-, Kjeller, Norway
[c]Washington University, MO, USA
[d]Departamento de Ingeniería Química, Universidad Complutense de Madrid, 28040 Madrid, Spain

Abstract

Polysilicon production costs contribute approximately to 25-33% of the overall cost of the solar panels and a similar fraction of the total energy invested in their fabrication. Understanding the energy losses and the behaviour of process temperature is an essential requirement as one moves forward to design and build large scale polysilicon manufacturing plants. In this paper we present thermal models for two processes for poly production, viz., the Siemens process using trichlorosilane (TCS) as precursor and the fluid bed process using silane (monosilane, MS). We validate the models with some experimental measurements on prototype laboratory reactors relating the temperature profiles to product quality. A model sensitivity analysis is also performed, and the effects of some key parameters such as reactor wall emissivity, gas distributor temperature, etc., on temperature distribution and product quality are examined. The information presented in this paper is useful for further understanding of the strengths and weaknesses of both deposition technologies, and will help in optimal temperature profiling of these systems aiming at lowering production costs without compromising the solar cell quality.

Keywords: CVD reactors, Polysilicon, Solar Grade Silicon, Siemens process, Fluidized Bed Reactor, CFD Modelling

1. Introduction and scope

In the last years production of solar cells has by far surpassed microelectronics as the main consumer of polysilicon in the world market [1]. Although the exponential growth in world production capacity made the

---

*Corresponding author. Tel.:+34 91 453 35 49; fax:+34 91 544 63 41.
[1]*Email Address:* alba.ramos@ies-def.upm.es (A. Ramos)

silicon prices drop dramatically, they are foreseen to become stable in the next years [2, 3] and significant growth in polysilicon consumption is expected in the medium-long term [4, 5]. As the production of silicon feedstock is responsible of about 25-33% of the energy cost of an installed silicon based solar cell module [6, 7], the importance for polysilicon producers to reduce production costs is revealed [8].

The most common means of obtaining polycrystalline solar grade silicon (SoGSi) is via decomposition of a silicon containing reactant gas through heating. The currently favoured method is the chemical route from trichlorosilane (TCS), named the Siemens process, which leads to high quality polysilicon at the expense of high energy consumption. Thus, low-cost technologies of obtaining polycrystalline silicon are coming on the scene: i. e. monosilane (MS) based fluidized bed reactors (FBR). In short, at present two main trends in polysilicon production exist: increase efforts to reduce the ratio kilowatts-hour per kilogram (kWh/kg) of polysilicon produced through the traditional process and support the new low-cost technologies development to make the lower energy consumption a sufficient advantage compared to other process disadvantages [9].

1.1. Scope

CVD processes are complex; thermodynamics, radiation, fluid-dynamics, kinetics and chemistry are involved [10, 11, 12, 13]. Understanding of the fundamental reactions and how they influence product quality at the same time as to comprehend the phenomena responsible of the energy consumption, is key in order to aid further development in polysilicon CVD.

Although a debate in the polysilicon community about the benefits and drawbacks of these different deposition technologies exists [1, 2], there is a lack of reliable data, based on rigorous models, and contrasted experimentally in similar conditions [14, 15, 16]. Also, some of the shortcomings of the FBR in terms of material quality are related to the nature of the process. In this paper theoretical models of heat losses of a Siemens reactor and a FBR prototype are developed and the thermal distributions within a fluidized bed and a Siemens reactor are explored; both experimental data and associated modelling are presented. The thermal conditions within the reactors are directly linked to the decomposition and deposition sequence which in turn influences the quality of the produced silicon. Any reduction in silicon price cannot come at the expense of a reduction in solar cell performance. It is therefore essential to know how the thermal distribution is within different reactor concepts and how these distributions may be altered in order to promote favourable growth and suppress competing unwanted mechanisms.

As has been established earlier by others, the solar cell efficiency will ultimately depend on the concentration of impurities in the material, not to disregards other defects and the passivation of the surfaces [17]. Of these contributions the impurity concentration level is linked to the feedstock route while the other

2

contributions are linked to the crystallisation and cell processing. The question is therefore not if impurities may influence the possible obtainable efficiency of the solar cells, but if these levels are relevant as current limitation for the efficiency. A further question may be that for high efficiency cell concepts if sufficient material quality is obtainable through low cost routes.

2. Polysilicon deposition technologies

2.1. Siemens process

The traditional route for polysilicon production consists of chemical vapour deposition (CVD) from TCS [18]. CVD of polysilicon comprises two main steps: metallurgical silicon (MG Si) transformation to TCS and purification, and TCS reduction into high purity silicon. The latter, the CVD of polysilicon itself, is the largest contributor to the energy consumption of the overall process which is in the range of 45-80 kWh/kg; the best number corresponds to large capacity plants [19, 20, 21]. From now on, we refer to the CVD of polysilicon as the Siemens process.

The Siemens process occurs inside a bell reactor containing heated silicon rods in a reactive gas atmosphere. It requires high deposition temperatures while keeping the reactor wall relatively cold. Joule's effect is responsible of the heating of the rods until the deposition temperature, that is typically, 1100-1150°C. The initial diameter of the seed rods is less than 1 cm and the deposition process runs until rods diameters are in the range 13-20 cm. The need for maintaining large temperature differences between the deposition surfaces and the reactor wall -to avoid homogeneous nucleation that would lead to lower quality of the resulting material- will cause a limit to theoretical reactant yield; and is the main responsible of the high energy consumption. However, several improvements have been made to the design resulting in a substantial reduction in energy consumption [22].

The Siemens process was initially developed to produce electronic grade polysilicon (EG Si), which has a purity of at least 99.9999999%, or 9N. This is the purity level needed in the microelectronics industry, though the purity requirements in the solar PV industry may be less demanding [23, 24], what opens opportunities for possible modifications to reduce the energy consumption of the Siemens process.

2.2. Fluidized bed reactors

The most valued alternative to the Siemens reactor is the fluidized bed reactor (FBR) [25]. A cylindrical reactor vessel is filled with tiny silicon particles which are kept fluidized by an ascending gas flow, typically hydrogen. The column of particles in the fluidized bed is heated above 600°C for the decomposition reaction to occur and the reactive gas, monosilane gas (MS), is inserted. The initial diameter of the silicon particles

is in the range of microns, and after some dwelling time the particles have grown to a size suitable for extraction [26, 27].

In the FBR, the decomposition reaction to polysilicon deposition occurs at temperatures significantly lower than in a Siemens reactor. The FBR holds the potential to become the dominating CVD reactor for production of solar grade silicon since the energy consumption per kilogram of silicon produced is estimated to be in the range of 4-16 kWh/kg [28, 29]; numbers vary depending on the number of steps or energy consuming processes that have been accounted for its calculation. However, it is first necessary to address the challenges with purity and porosity, production of fine dust (fines), and to achieve good gas and temperature control, among others [30, 31].

The purity of the polysilicon obtained from MS in a FBR is below that of the Siemens process, compromising its use for microelectronic devices. It can be acceptable for solar cells, provided good temperature control and low amount of fines formation achieved in the process [32, 33].

3. Heat loss phenomena in SoGSi production

First, the heat loss problem associated with polysilicon CVD is addressed; all contributions to the energy consumption of both the Siemens reactor and the FBR are introduced. When applying the energy balance equation to the polysilicon CVD problem, the following contributions must be evaluated: the rate of variation of energy, the net rate of kinetic and internal energy transfer by convective transport, the net rate of heat transfer by conduction due to temperature gradient and enthalpy transport for an ideal gas, the rate of work done on the system by other molecular transport mechanism (pressure and stress) and by external forces, the heat of chemical reactions and the heat transfer by radiation [34, 35, 36]. In the following, the relevant terms contributing to the energy consumption of each particular reactor will be identified.

3.1. Siemens reactor

In the Siemens reactor heat loss is due to radiation, conduction and convection via gases and the heat consumed due to the chemical reactions taking place [37]. Of these, the major contributor is radiation heat loss [38]; contribution of the latter is typically below 1%, thus heat consumption due to chemical reactions taking place can be disregarded.

As stated above, the main challenge of the Siemens process is to reduce the ratio kWh/kg of silicon produced. On the one hand, faster deposition processes are desired to reduce this ratio. On the other hand, higher deposition rates are obtained with higher temperatures, leading to higher energy consumption.

4

Therefore, a compromise solution is needed; it is widely accepted that the deposition temperature at which the ratio kWh/kg is minimized is between 1100-1150°C [39].

3.2. FBR

Several attempts have been made to use chlorosilanes in fluidized beds for polysilicon production. However, this has so far proven challenging as there will always be a temperature distribution within a fluidized bed. This is simply because the reactant needs to be injected at a temperature below its decomposition temperature: for both TCS and MS this will typically be below 300°C. Ideal deposition temperature will be 600-800°C for MS, for TCS it will be 900-1100°C [31, 12]. However, whereas suboptimal deposition due to low temperature may lead to hydrogen inclusions for silanes, they will lead to chlorine inclusions for chlorosilane based depositions [40]. This may be improved by going to higher temperatures and higher hydrogen to TCS ratios, as these will increase reverse mechanisms leading to continual chlorine removal. However this will directly go against the motivation for using FBRs since these two factors will lead to higher energy consumption. In the end, for TCS feed in FBR, it will not be possible to come down to the low energy consumption possible with silane based reactors merely due to the fundamental kinetics.

In case of FBRs radiation and the heat transfer due to mass transport are both important contributors to the energy consumption. The process of silane decomposition into elemental silicon and hydrogen is weakly exothermic. However, not all intermediate reactions are exothermic so the decomposition may not give a net heat contribution in all parts of the reactor. The layout of the reactor and the hydrogen to silane ratio will therefore be important in how low energy consumption will be possible.

4. CVD reactors modeling

The process of conversion of TCS gas to solid polysilicon (Siemens CVD) has been investigated in a computational model, as is the process of conversion of MS gas to solid polysilicon (FBR). Due to the configuration of both reactors, the CFD models developed are well represented by axi-symmetric models. The global model accounting for all important aspects of heat transfer and gas flow has been developed using SiSim [41, 42, 43], a software dedicated to silicon production processes developed in the frame of the Norwegian center Solar United. For general 3D problems, the dependent variables are the velocities u, the pressure p, the temperature T and the radiosity J. These time-dependent variables are solved from the incompressible Navier-Stokes equations including the continuity equation, the energy conservation equation

and the surface-to-surface radiation model. Model equations for mass and momentum conservation are

$$\frac{\partial u_i}{\partial x_i} = 0 \tag{1}$$

and

$$\frac{\partial u_i}{\partial t} + u_j \frac{\partial u_i}{\partial x_j} = -\frac{1}{\rho_0} \frac{\partial p}{\partial x_i} + \frac{\rho - \rho_0}{\rho_0} g_i + \frac{\partial}{\partial x_j}(v \frac{\partial u_i}{\partial x_j}) \tag{2}$$

In equation 2, g is the gravitational acceleration, t is the time, ρ is the density, ρ_0 is the reference density, v is the molecular kinematic viscosity and x_i is the spacial coordinate in direction i. The conservation of energy equation is employed to calculate the temperatures. This equation reads

$$\rho c_p \frac{\partial T}{\partial t} + \rho c_p u_j \frac{\partial T}{\partial x_j} = \frac{\partial}{\partial x_j}(\lambda \frac{\partial T}{\partial x_j}) \tag{3}$$

where c_p is the specific heat capacity and λ is the thermal conductivity. Thermal radiation is the main heat transfer mechanism in CVD reactors. The surface-to-surface radiation model is used to calculate thermal radiation [44, 45]. This model makes use of view factors (F_{ij}). These are geometrical parameters that define the fraction of radiation leaving surface i, which is intercepted by surface j. View factors are calculated using the hemicube method [46]. Radiosity has the units W/m^2, and it accounts for all of the radiant energy leaving a surface. The governing equation reads

$$J_i = \varepsilon_i \sigma T_i^4 + (1 - \varepsilon_i) \sum_{j=1}^{n} F_{ij} J_j \tag{4}$$

where J_i represents the radiosity of surface i, ε_i represents the emissivity of surface i and σ is the Stefan-Boltzman constant equal to $5.67 \cdot 10^{-8}$ W/(m$^2 \cdot$ K^4). For gas flow at solid surfaces, a non-slip boundary condition is used for the velocities. For the thermal radiation model, the element surface temperatures calculated from the previous time step -initial temperatures if the current time step is the first- constitute the boundary condition. The coupling between the thermal radiation model and the energy conservation equation is done as follows. Once the radiosities are known from equation 4, the boundary heat flux of each element surface is calculated from

$$q_i = \frac{\varepsilon_i \sigma T_i^4 - \varepsilon_i J_i}{(1 - \varepsilon_i)} \tag{5}$$

This heat flux serves as a thermal boundary condition in the subsequent thermal analysis of the solids.

4.1. Siemens laboratory scale reactor

The Siemens laboratory reactor consists of a cylindrical chamber in which one or more rods are fixed. The seed silicon rods are heated by the Joule effect by means of a power supply through a pair of electrodes;
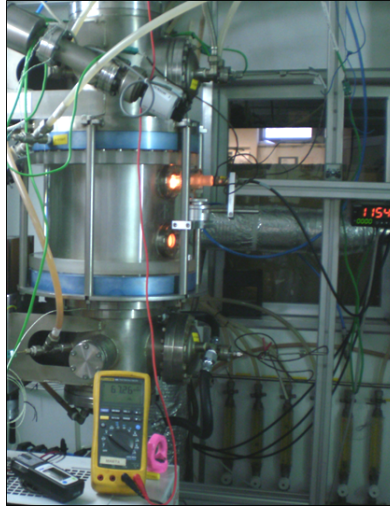
Figure 1: Siemens laboratory reactor.

placed at the top and bottom of the cylindrical chamber. The reactor wall is kept at low temperatures by means of water cooling. The reactive gases enter the reactor chamber through the bottom, flow along the rod or rods placed inside, and leave through the top. In figure 1 a photograph of the Siemens laboratory reactor is presented. Temperatures at a number of log points and at the rods' surface are monitored during a deposition experiment. In addition, inlet gases mixture, pressure, gas flow and the power supplied are monitored. The initial rods' diameter is 7-8 mm and the deposition experiments length is typically 8-10 hours. Detailed information of the Siemens prototype set-up and data of a number of experiments can be found in [47, 48].

4.1.1. Model

The geometry and the mesh of all elements conforming the laboratory reactor are developed. The length of the silicon rod is 53 cm and the inner diameters of the reactor chamber are 20 and 15 cm. The different domains defined are: the rod (silicon), the casing (stainless steel), the fluid flow domain (hydrogen and TCS) and the cooling (water). Finally, the mesh is composed of 3836 elements and 4722 nodes.

4.1.2. Results

Three different experiments conducted in the laboratory reactor were selected to be reproduced by means of CFD modelling. These experiments present a single rod configuration and are conducted at approximately 1000, 1100 and 1150°C; experiments A, B and C, respectively. Conditions of pressure and inlet gas composition are the same for the three experiments. Although obvious differences in the simulated results for
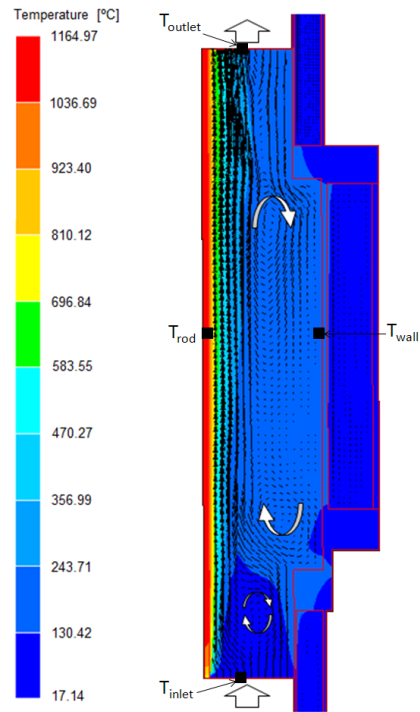
7

Figure 2: Temperature distribution and fluid flow field (black arrows) of the Siemens laboratory reactor.

these three cases are obtained -maximum temperatures or gas velocities-, the fluid flow and the temperature fields obtained resemble each other. As an example, in figure 2 the temperature distribution and the fluid flow field corresponding to experiment C -for a 8 mm diameter rod at steady state- are shown. The different colors correspond to the temperatures distribution and the black arrows indicate the magnitude and direction of the gas flow. The higher temperatures are reached at the rod, 1164°C, the inlet gas temperature is 50°C, the outlet gas temperature is 281°C, the wall temperature at the middle part of the reactor chamber is 293°C and the temperatures of the external wall are around 20°C due to the water cooling. By looking at the flow field it can be observed that gas recirculation zones exist; the sudden expansion and contraction of the chamber are the factors that create the recirculation zones. Notice that in the laboratory scale reactor the wall temperature is far below the critical one, but in the industry the inner wall temperature can reach much higher temperatures, then it is forced -by water cooling- to be below 400-500°C to avoid undesired high temperature regions.

In tables 1, 2 and 3, experimental temperatures measured at a number of points in experiments A, B and

8

Table 1: Temperatures measured and modelled for experiment A, and relative difference among them.

	Experimental	Modelling	Difference
T_{rod} [°C]	1002	978	2.3 %
T_{wall} [°C]	-	139	-
T_{inlet} [°C]	52	50	3.8 %
T_{outlet} [°C]	210	219	4.2 %

Table 2: Temperatures measured and modelled for experiment B, and relative difference among them.

	Experimental	Modelling	Difference
T_{rod} [°C]	1101	1083	0.5 %
T_{wall} [°C]	-	225	-
T_{inlet} [°C]	50	50	0.0 %
T_{outlet} [°C]	224	251	12.0 %

C are compared with the simulation results. Since the power supplied is an input for the simulations, both, experimental and simulated numbers are coincident. The power input for experiments A, B and C is 1700, 2023 and 2363 W, respectively.

From the comparison of the values presented in tables 1, 2 and 3 a good agreement is found between experimental and simulation data. For example, the differences in the rod temperature are 24, 18 and 6°C, respectively. A two-colour pyrometer is used for the experimental measurement of the rod temperature; its measurement error can be up to ±2°C. The other temperature measurements are conducted with thermocouples, which error is considered to be within ±10°C. The fluid flow domain does not match exactly the reality but it is quite close; the difference between the measured and modelling results is explained because in the real case the gases are fed in and extracted from the reactor chamber horizontally instead of vertically. Finally, the wall temperature was not recorded, but the modelling results are shown since it is considered an important parameter.

The experimental growth rates obtained for experiments A, B and C are 2.1, 3.4 and 3.9 μm/min. These values lead to several times higher energy consumption than in industry: the ratio kWh/kg obtained with the

Table 3: Temperatures measured and modelled for experiment C, and relative difference among them.

	Experimental	Modelling	Difference
T_{rod} [°C]	1158	1164	0.5 %
T_{wall} [°C]	-	293	-
T_{inlet} [°C]	52	50	3.8 %
T_{outlet} [°C]	253	281	11.0 %

Table 4: Wall emissivity sensitivity analysis for conditions of experiment B.

Wall emissivity [-]	0.3	0.6	0.85
T_{rod} [°C]	1135	1083	1048
T_{wall} [°C]	247	225	149
T_{inlet} [°C]	50	50	50
T_{outlet} [°C]	264	251	234

laboratory prototype are in the range of 350-400. The bad compactness of the single-rod configuration, the process pressure -which is 6 times lower than in industry [19]- and the low percentage of TCS -2% vol.-, explains this high energy consumption.

4.1.3. Sensitivity analysis

From the results presented above, the CFD model developed for the Siemens laboratory scale reactor is found to be good enough to reproduce the polysilicon deposition process conditions. The difference between the predicted and measured temperature of the rod is below 2.3%.

Here, the model is applied to the study of the effect of the variation of the wall emissivity on the temperature distribution. Experimental deposition conditions of experiment B are considered and different wall emissivities are simulated. In table 4 the relevant temperatures resulting from the simulation for wall emissivity values of 0.3, 0.6 and 0.85 are presented. It can be observed that for the same power input reduced emissivities lead to higher rod surface temperatures, while increased emissivities lead to lower ones. The temperatures of the wall and the outlet gases also increase as the rod temperature does. Notice that the condition of the surfaces within the reactor can change during a deposition process -thus, also the emissivities-. As exposed in section 3, higher rod temperatures imply faster deposition processes; thus low wall emissivities are desired in order to decrease the ratio kWh/kg of polysilicon. However, this consumption reduction would be limited by the final material quality if nucleation temperatures are reached.

Moreover, the effect of different inlet flow rates on the fluid flow and the temperature distribution is studied. All deposition process conditions of experiment B are reproduced considering gas speeds at the reactor inlet two and four times larger. In table 5 the relevant temperatures predicted by the simulation for inlet flow rates of 15, 30 and 60 standard litres per minute (slm) are presented. It can be observed that as the flow rate increases the temperatures of the rod, the wall, and the outlet gases decreases, since convection and conduction heat loss via gases increase with the flow rate. Higher flow rates would lead to higher deposition rates if the process is limited by mass transport. Thus, higher flow rates would be desired in order to reduce the ratio kWh/kg consumed until the process becomes to be limited by the reaction. Most likely deposition

10

Table 5: Flow rate sensitivity analysis for conditions of experiment B.

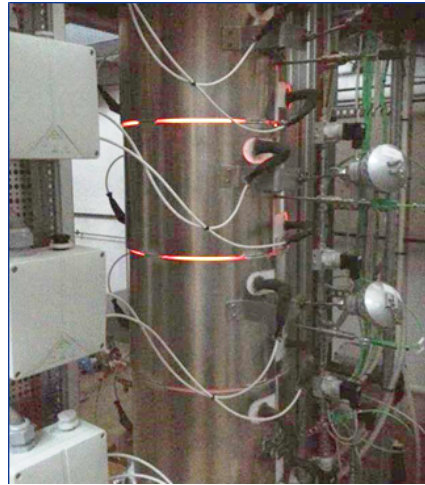| Flow rate [slm]	15	30	60
T_{rod} [°C]	1083	1079	1067
T_{wall} [°C]	225	220	204
T_{inlet} [°C]	50	50	50
T_{outlet} [°C]	251	224	187

Figure 3: FBR prototype reactor.

rates would be mass transfer controlled due to the high temperatures [36, 49].

4.2. FBR prototype reactor

The FBR prototype consists of a cylindrical chamber in which the silicon beads are deposited. The gas enters the reactor chamber through the bottom part, through a number of holes machined on the baseplate, and the gas, together with the silicon beads, is heated by means of four heaters surrounding the cylindrical chamber. In figure 3 a photograph of the FBR prototype is shown. The typically initial beads diameter is 200 μm. The fluidizing gas can be either nitrogen, hydrogen or a mixture of both. Once a good fluidization is achieved and the deposition temperature reached, the reactive gas -MS- is introduced and the decomposition starts. MS concentration varies in the range of 5-20%, and the inlet flow rates are tipically between 30-130 slm. The length of the deposition processes conducted with the prototype is between 8-25 h. Further information and data about the FBR prototype can be found in [50, 51].

11

4.2.1. Model

The geometry and the mesh of all elements conforming the FBR prototype are developed. The height of the reactor chamber is 150 cm and its inner diameter is 15.5 cm; The heated length is around 100 cm. The different domains defined are: the baseplate (aluminium, synthetic wool and stainless steel), the casing (stainless steel), the fluid flow (hydrogen and MS), the heaters (induction coil), the wall isolation (ceramic foam) and the cooling (water). Finally, the mesh is composed of 14272 elements and 15912 nodes.

The FBR prototype modelling is more complex than the laboratory Siemens reactor and it has the limitation that the silicon beads are not part of the thermal model. This would require a tailor-made sub-model for handling a large number of dynamic particles that interfere. These particles consume energy which in our modelling approach is distributed to the reactor solids. Notwithstanding, the radiation, thermal and fluid flow problems can be defined; and by solving these problems the temperature distribution and the fluid flow field -among others- are obtained. Notice that the fluid flow field resultant of this model will not be close to reality, neither the power consumed to obtain the temperature distribution measured experimentally, since the silicon beads are not modelled. However, main challenges of the FBRs are directly dependent on gas temperature distribution, thus, highly relevant information can be obtained if the modelled temperature distribution is consistent with the experimental data even with this simplified version of the fluidized bed model.

4.2.2. Results

Results of the FBR prototype modelling are compared with experimental data. In this case, two different experiments conducted with the FBR prototype are selected: experiments D and E. All boundary conditions in both experiments, except the inlet flow rate, are similar (decomposition temperatures, pressure, gases mixture, etc.). The inlet flow rate in experiments D and E is 30 and 120 slm, respectively. From these experiments, temperature measurements at a number of points have been monitored; these points are indicated in figure 4. The temperature distribution shown in figure 4 corresponds to experiment D. In tables 6 and 7 measured and simulated values are compared. In both experiments, differences between experimental and simulation data are below 5% for almost all the gas temperature measurements. In table 6 a good agreement is found for the reactor wall temperatures, while higher differences between the measured and the calculated data are found in the lower part of the reactor. In table 7 the opposite occurs, there is a good agreement between the temperatures at the bottom part of the reactor but higher differences in between measured and calculated data are obtained at the reactor wall.

Due to the choice of applying a axi-symmetrical model, the reactor baseplate geometry deviates from the
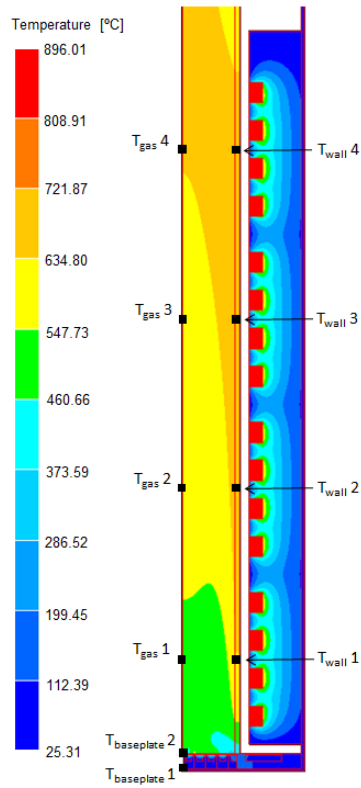
Figure 4: Temperature distribution of the FBR prototype reactor in experiment D.

Table 6: Temperatures measured and modelled for experiment D, and relative difference among them.

	Experimental	Modelling	Difference
$T_{baseplate}$ 1 [°C]	51	46	9.8 %
$T_{baseplate}$ 2 [°C]	631	518	17.9 %
T_{gas} 1 [°C]	627	520	17.0 %
T_{gas} 2 [°C]	627	596	4.9 %
T_{gas} 3 [°C]	628	624	0.6 %
T_{gas} 4 [°C]	628	636	1.3 %
T_{wall} 1 [°C]	585	603	3.8 %
T_{wall} 2 [°C]	649	647	0.3 %
T_{wall} 3 [°C]	686	653	5.0 %
T_{wall} 4 [°C]	688	650	5.2 %

Table 7: Temperatures measured and modelled for experiment E, and relative difference among them.

	Experimental	Modelling	Difference
$T_{baseplate}$ 1 [°C]	50	53	6.0 %
$T_{baseplate}$ 2 [°C]	571	582	2.1 %
T_{gas} 1 [°C]	598	586	2.0 %
T_{gas} 2 [°C]	613	595	4.5 %
T_{gas} 3 [°C]	624	621	0.5 %
T_{gas} 4 [°C]	703	665	5.4 %
T_{wall} 1 [°C]	496	557	12.3 %
T_{wall} 2 [°C]	654	748	14.3 %
T_{wall} 3 [°C]	704	825	17.1 %
T_{wall} 4 [°C]	758	883	16.4 %

real one. The holes where the gas enters the reactor are approximated by inlet ring areas in the model. This difference is noticeable for low inlet gas flow, and it explains the higher differences between the temperatures in the lower part of the reactor in experiment D. In addition, since the silicon beads are not simulated, considering a slower gas flow the differences of the real and the simulated heat transfer coefficient -between the reactor wall and the fluidized bed- is closer. The latter explains the higher differences in the wall temperature obtained in experiment E. The maximum differences obtained in experiment D expressed in Celsius degrees are 113°C ($T_{baseplate2}$). In experiment E differences of the wall temperatures expressed in Celsius degrees are higher, in the range of 61 to 125°C. All experimental temperature measurements are conducted with thermocouples, which error is considered to be within ±10°C.

4.2.3. Sensitivity analysis

The results presented above show that the CFD model developed provides reasonable estimates of the temperatures distribution.

Table 8: Flow rate sensitivity analysis for conditions of experiment E.

Flow rate [slm]	70	120	150
$T_{baseplate}$ 1 [°C]	54	53	53
$T_{baseplate}$ 2 [°C]	585	582	582
T_{gas} 1 [°C]	588	586	586
T_{gas} 2 [°C]	645	595	584
T_{gas} 3 [°C]	728	621	585
T_{gas} 4 [°C]	784	665	598
T_{wall} 1 [°C]	558	557	547
T_{wall} 2 [°C]	776	748	707
T_{wall} 3 [°C]	878	825	811
T_{wall} 4 [°C]	906	883	871

The influence of a number of the relevant parameters in the polysilicon deposition by means of the FBR prototype are then studied: gas mixture, heat transfer between interfaces, inlet flow rate and material properties. Different gas composition for the same process conditions were simulated: mixtures from 5 to 30% of MS and hydrogen; in all cases the temperature distribution obtained was virtually identical. Heat transfer coefficients between the different interfaces were also varied -within the known orders of magnitude for each one- and no relevant differences in the resultant temperature distribution were obtained.

The effect of the flow rate in the temperature distribution is strong. For the deposition conditions of experiment E, a few simulations considering different flow rates are conducted. In table 8 the temperatures at a number of positions in the reactor for different flow rates -70, 120 and 150 slm- are shown. It can be observed that as the flow rate is increased, the temperatures at the monitoring points are reduced. In addition, the effect of considering different flow rates observed is stronger as we move far from the base plate. Notice that this effect will not be so strong if a good fluidization of the bed is achieved.

Some of the materials considered for the FBR prototype assembly could be changed for more proper ones if the material properties are found to be relevant for changing the temperature distribution to a better one. In order to perform this sensitivity analysis the following material properties are selected: the reactor wall emissivity and the thermal conductivity of the baseplate.

In table 9 the temperatures at a number of points for different wall emissivities -0.2, 0.5 and 0.8- are shown. If the wall emissivity is increased from 0.5 to 0.8, all temperatures in table 9 increase: the average of this increment is 3.7% (or 23.0°C). When decreasing the wall emissivity from 0.5 to 0.2, all the temperatures decrease; now, the average of this decrement is 4% (or 25.9°C). For all data in table 9 the same power input has been considered, thus, for a selected deposition temperature, higher wall emissivities lead to lower

Table 9: Wall emissivity sensitivity analysis for conditions of experiment D.

Emissivity [-]	0.2	0.5	0.8
$T_{baseplate}$ 1 [°C]	45	46	48
$T_{baseplate}$ 2 [°C]	497	518	543
T_{gas} 1 [°C]	502	520	547
T_{gas} 2 [°C]	576	596	623
T_{gas} 3 [°C]	594	624	645
T_{gas} 4 [°C]	598	636	652
T_{wall} 1 [°C]	580	603	610
T_{wall} 2 [°C]	619	647	675
T_{wall} 3 [°C]	624	653	681
T_{wall} 4 [°C]	624	650	678

energy consumption while lower emissivities do the opposite. No relevant differences in the temperature distribution are noticed; differences between the maximum and minimum gas temperatures changing the wall emissivities from 0.8 to 0.2 are under 5%. Hence, lower wall emissivities lead to a small improvement of the temperature homogeneity, and at the same time lower energy consumption (see 4.1.3).

Finally, the thermal conductivity (λ) of the baseplate insulation element has been increased 4 and 8 times. In figure 5 the temperature distribution of the baseplate for the different λ -0.08, 0.32 and 0.64 W/K·m- is shown. It can be clearly appreciated how as the thermal conductivity increases the temperature gradient decreases. The noticeable changes in the temperature distribution of the baseplate only affect significantly the gas temperatures at the very bottom of the fluidized bed; lower λ leads to higher temperatures in this region. Therefore, lower λ could be considered in order to increase the undesired low temperatures of the gas region close to the baseplate; that favour homogeneous nucleation -thus, fines formation- [51].

5. Discussion

CVD Polysilicon quality directly affects the solar cell performance. Despite a range of accepted purities of the raw material for solar cells production exist, the higher material quality -up to a limit- the higher cell efficiency [52, 53, 54].

5.1. Siemens reactor

The CFD model for the Siemens laboratory reactor give us reliable data about the fluid flow, the temperatures distribution, and definitely, about the power consumption. Therefore, this model allows to identify the parameters responsible of the greatest power consumption and, thus, suggest some modifications that could decrease the ratio kWh/kg of silicon produced.
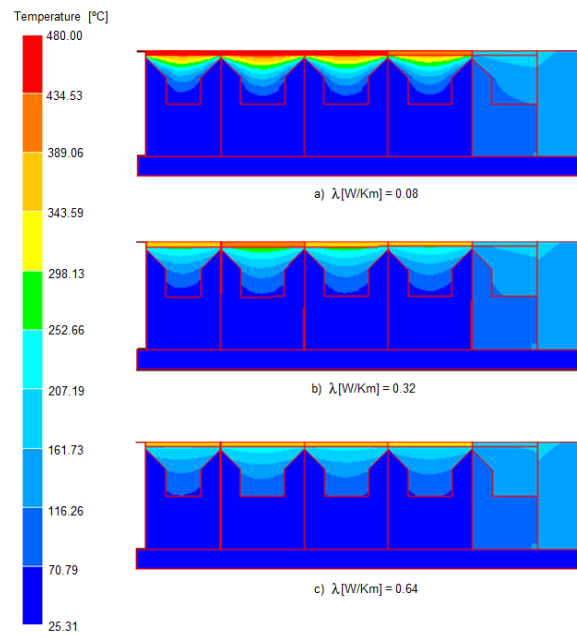
Figure 5: Temperature distribution of the FBR prototype baseplate for different thermal conductivities of the isolation element. Deposition conditions of experiment D.

On the other hand, deposition temperature has an important effect on the output material quality. For polysilicon deposition from TCS in Siemens reactors, slower deposition processes (low deposition temperatures) lead to high quality material and smooth surface finishing. As the deposition temperature increases the growth rate does the same, thus the increment of the deposition rate leads to greater surface roughness. Above a certain deposition temperature (typically above 1150°C) dendritic growth starts [47] and risk of homogeneous nucleation exists [31]. Now, growth rates are faster but the quality of the output material is lower.

From the modelling results and the sensitivity analysis presented in subsections 4.1.2 and 4.1.3, a high reflective reactor wall leads to higher deposition temperatures for a fixed power input, therefore the ratio kWh/kg can be reduced. The output material quality will be lower, but in most cases enough to fulfil the purity required for the photovoltaic industry. The key to obtain a high purity polysilicon is to keep the reactor wall at low temperatures, below 400-500 °C to avoid nucleation phenomenon [55].

5.2. FBR

For the FBR, the CFD model give us reliable data about the temperatures distribution, that is related to material quality. The FBR modelling has been performed with a relatively simple model compared to other approaches. Several mechanisms active within a FBR have not been taken into account. However, the data fits closely with the experimental results. Considering the same reactive gas, FBR has advantages over a fixed bed or other CVD-type reactors. FBR presents more homogeneous temperature and concentration profiles, gradients are avoided, due to the fluidization mixture effect. The better homogenization avoids hot or cold points in the particles bed inside the reactor chamber. However, temperature gradients appear in between the bed and the surrounding elements, baseplate or reactor wall. These gradients will depend on a number of factors but in general the temperature differences in relation to the efficiency of the heat transfer mechanisms will dictate the temperature distribution. The distribution is crucial as the decomposition sequence of silane to silicon contains a number of intermediate temperature dependent reactions [9]. Further, the fluid-mechanics of the bed will also influence the nature of the growth. Larger bubbles in silane rich regions of the bed will promote gaseous nucleation and homogeneous growth thus fines production. Fines production is directly a problem because it is a loss mechanism, even if some of the fines may be scavenged and thus not directly lost [30]. However, this contribution comes with a cost since fines scavenging may lead to porous regions, and hydrogen inclusions [50, 56, 57]. To a large extent it is possible to overcome these challenges by limiting the mean bubble size, limit the silane concentration and maintain the right temperature profile close to the silane inlet of the FBR [50]. The experimental data presented in this paper together

18

with the modelling tool may be one step towards a tool to describe the reactant inlet thermal profile for various designs and thus aid further design work for such reactors.

5.3. CVD reactors comparison

When comparing between the Siemens reactor and the FBR for polysilicon production, in terms of energy consumption, the alleged advantages of the FBR -such as lower energy costs due to lower deposition temperatures- are not due to the FBR itself, but to the use of MS gas instead of TCS. To some extent this argument may be true. The two have about the same decomposition initiation temperature around 400°C but a very different deposition temperature -for TCS in the order of 850-1100°C whereas for silane 650-700°C-; this means that the actual temperature difference needed will be larger for TCS which is directly linked to the thermal losses. Also, for TCS the maximum theoretical yield is in the order of 23% while the value achieved in practise is around 15%, which means that one needs to heat and recycle another 85% which does not contribute to the production. Lastly hydrogen takes place in the decomposition reaction for TCS which means that one needs to have a large excess hydrogen flow to keep the reaction going.

The advantage of the FBR is most obvious for the silane based process [58]. For silane the same mechanisms may lead to hydrogen encapsulation, however, hydrogen may be removed from the silicon lattice by heating to a temperature far below the melting point [12]. Hydrogen encapsulations will therefore not directly reduce the bulk minority carrier lifetime, which will be different for chlorine encapsulations typical of TCS in a FBR.

The largest difference between the two reactor types is the heat transport mechanisms in comparison to the transport of the reactant. For a Siemens type reactor the dwelling time of silane may be relatively long as the gas may be in parts of the reactor with a too low temperature and the heat transport through radiation is quite effective due to the large temperature differences and that the different surface are exposed in relation to each other. For a FBR the situation is quite different, if the bubbles are kept small. The reactant is quite quickly heated to the point of decomposition upon being inserted to the reactor. The different surfaces are not directly exposed to each other which means that direct radiation is lower than for the Siemens layout. The success of the reactor therefore lies in how to limit the heat transport between the surfaces of different temperature while at the same time maintaining an ideal temperature profile in the reactant inlet area in order to aid a controlled bead initiated growth and suppress formation of fines and subsequently fines scavenging and porous regions [12, 9]. There is also an inherent challenge in the combined fluid-mechanics and the wear on the internal surfaces of the FBR. This mechanism may to a large extent be overcame by controlling

19

the fluid mechanics, use of liners and maintaining a layer of protective silicon on the internal reactor surface. It is nevertheless a challenge with FBR which needs to be addressed.

6. Conclusion

The Siemens process has been until now the main polysilicon production process. The high energy consumption of this type of reactors and the market context make low cost technologies -like FBR- coming into scene. However, FBRs need first to overcome a number of challenges to make their lower energy consumption a sufficient advantage compared to process disadvantages. For both type of reactors the nature of the deposited silicon will depend on among other things the temperature of the deposition surface at the time of deposition. The structure of the material, the crystallinity, the porosity and also the possibility of chlorine encapsulations for chlorosilane based reactors and hydrogen encapsulation for silane based reactors. For the Siemens layout the challenge is limited since the deposition temperature to a large extent may be closely controlled. For the FBR there will allways be a distribution in deposition temperature since the history of the individual beads meeting the incoming reactant will be different. This challenge is generic for the layout type and the only thing one may do is to limit the problem to a point where the result is minor.

The CFD models for the Siemens and FBR prototypes developed give us reasonable estimates of the temperature distribution, therefore they become an important tool for further understanding of the basic reactor design aspects of these processes and will help in optimal temperature profiling of these systems. The reactant thermal profile is key to understand how the fundamental reactions influence the product quality, and the models presented give relevant insight to address this issue.

20

References

[1] K. Hesse, E. Schindlbeck, E. Dornberger, M. Fischer, *Status and Development of Solar-Grade Silicon Feedstock,* 24th European Photovoltaic Solar Energy Conference (2009) pp. 883-885.

[2] M. Meyers, *Silicon 2012: The New Si Game*, 10th Solar Silicon Conference, 2012.

[3] Yijun Liu, Yingqi Liu, *The industrial research about China solar PV based on the price of polysilicon*. Advanced Materials Research, Vol. 383-390 (2012) pp. 7043-7048.

[4] R. Steemana, J. Yonga, Ø. Mjøsb, A. Songb, *Integrating the Value Chain: The Impact of Silicon Quality on Cell Performance*, Energy Procedia Vol. 15 (2012) pp. 20-29.

[5] J. Bernreuter, *The polysilicon market - Perspectives on Demand, Supply and Production Technologies*, Silicon for the Chemical and Solar Industry XI (2012) pp. 281-284. 07).

[6] B. Ceccaroli, O. Lohne, *Handbook of Photovoltaic Science and Engineering, in: Solar Grade Silicon Feedstock*, 2nd Edition, 2011, pp. 169-217.

[7] E. Alsema, M. de Wild-scholten, *Reduction of the environmental impacts in crystalline silicon module manufacturing*, 22nd European Photovoltaic Solar Energy Conference and Exhibition (2007) pp. 829-836.

[8] T. F. Ciszek, *Photovoltaic materials and crystal growth research and development in the gigawatt era*, Journal of Crystal Growth, Vol. 393 (2014) pp. 2-6.

[9] W. O. Filtvedt, A. Holt, P. A. Ramachandran, M. C. Melaaen, *Chemical vapor deposition of silicon from silane: Review of growth mechanisms and modeling/scale up of fluidized bed reactors*, Solar Energy Materials & Solar Cells 107 (2012) pp. 188-200.

[10] C. R. Kleijn, *Computational modeling of transport phenomena and detailed chemistry in chemical vapor deposition a benchmark solution*, Thin Solid Films 365 (2000) pp. 294-306.

[11] Z. Pan, *Effect of boundary layers on polycrystalline silicon chemical vapor deposition in a trichlorosilane and hydrogen system*, Chinese Journal of Chemical Engineering, 19(1), (2011) pp. 1-4.

[12] W. O. Filtvedt, M. Javidi, A. Holt, M. C. Melaaen, E. Marstein, H. Tathgar, P.A. Ramachandran, *Development of fluidized bed reactors for silicon production*, Solar Energy Materials & Solar Cells 94 (2010) pp. 1980-1995.

[13] L. Jianlong, C. Guanghui, Z. Pan, W. Weiwen, D. Jihai, *Technical Challenges and Progress in Fluidized Bed Chemical Vapor Deposition of Polysilicon*, Chinese Journal of Chemical Engineering, 19(5), (2011) pp. 747-753.

[14] P. Ege, A. Abbasi, J-S. Seo, J-S. Lee, J-H. Lee, *Fluidized Deposition Reactor for Silicon Production*, SolarCon China, 2012.

[15] A. Müller, R. Sonnenschein, T. Sill, A. Glz, C. Beyer, J. Piotraschke, D. Kaden, D. Bednarek, S. Stute, *The Sunsil-Process: The most energy-efficient process to produce solar grade silicon*, in: The 24th EUPVSEC, Hamburg, 2009.

[16] B. Ceccaroli, O. Lohne, E. J. Øvrelid, *New advances in polysilicon processes correlating feedstock properties and good crystal and wafer performances*, Phys. Status Solidi C 9, No. 10-11 (2012) pp. 2062-2070.

[17] J. R. Davis, A. Rohatgi, R. H. Hopkins, P. D. Blais, P. Rai-Choudhury, J. R. McCormic, H. C. Mollenkopf, *Impurities in Silicon Solar Cells*, IEEE Transactions on electronic devices, Vol 27 No 4. (1980) pp 677- 687.

[18] W. C. O'Mara (Ed.), R. B. Herring, L. P. Hunt, *Handbook of semiconductor silicon technology, in: Polysilicon preparation*, 1990, pp. 33-93.

[19] S. K. Chunduri, *Innovations in inertia: market survey on Siemens-type CVD reactors*, Photon International 4 (2013) pp. 114-126.

[20] Y. Delanoy, *Purification of silicon for photovoltaic applications*, Journal of Crystal Growth 360 (2012) pp. 61-67.

[21] J. Maurits, *Reducing polysilicon materials cost*, Photovoltaics International, 13th Edition, 2011.

[22] G. del Coso, I. Tobías, C. Cañizo, A. Luque, *Temperature homogeneity of polysilicon rods in a Siemens reactor*. Journal of Crystal Growth 299 (2007) pp. 165-170.

[23] Silicor Materials, *How did we revolutionize the solar industry?*, White paper, 2012.

[24] B. R. Bathey, M. C. Cretella, *Review solar-grade silicon*, Journal of Material Science, Vol. 17 (1982) pp. 3077-3096.

[25] W. W. Osborne, M. V. Spangler, L. C. Allen, R. J. Geertsen, P. E. Ege, W. J. Stupin, G. Zeininger, Assign. REC Silicon, *Fluid Bed reactor*, US 8.075.692 B2 (2011).

[26] W-C. Yang, *Handbook of Fluidization and Fluid-Particle Systems*, CRC Press, 2003.

[27] W. 0. Filtvedt, *Production of polysilicon from silane pyrolysis in a fluidized bed*, PhD Thesis, Telemark University College, Faculty of Technology, Norway, 2013.

[28] J. O. Odden, G. Halvorsen, H. Rong, R. Gløckner, *Comparison of the energy consumption in different production processes for solar grade silicon* , Silicon for the Chemical and Solar Industry IX, Norway, 2008.

[29] T. Torvund, CEO REC Silicon, *Granular polysilicon technology*, SNEC (2012) Shanghai, China.

[30] M. M. Dahl, A. Bellou, D. F. Bahr, M. G. Norton, E. W. Osborne, *Microstructure and grain growth of polycrystalline silicon in fluidized bed reactors*, Journal of Crystal Growth 311 (2009) pp. 1496-1500.

[31] C. S. Herrick, D. W. Woodruff, *The Homogeneous Nucleation of Condensed Silicon in the Gaseous Si-H-Cl System*, Journal of The Electrochemical Society: Solid-state Science and Technology (1984) pp. 2417-2422.

[32] B. Ceccaroli, O. Lohne, *Solar Grade Silicon Feedstock*, in: A. Luque, S. Hegedus (Eds.), Handbook of Photovoltaic Science and Engineering, John Wiley & Sons, 2nd edition (2010) pp. 169-217.

[33] B. E. Ydstie, J. Du, *Producing Poly-Silicon from Silane in a Fluid Bed Reactor*, in: L. Kosyachenko (Ed.), Solar Cells - Silicon Wafer-Based Technologies, InTech (2011) pp 125-138.

[34] R. B. Bird, W. E. Stewart, E. N. Lightfoot, *Transport Phenomena*, 2nd edition, John Wiley & Sons, New Jersey, 2007.

[35] F. Kreith, M. Bohn, *Principles of Heat Transfer*, 6th edition, Thomson, Stamford (2002) pp. 73-95.

[36] D. E. Rosner, *Transport Processes in Chemically Reacting Flow Systems*, Dover publications, New York, 2000.

[37] A. Ramos, A. Rodríguez, C. del Cañizo, J. Valdehita, J. C. Zamorano, A. Luque, *Heat losses in a CVD reactor for polysilicon production: Comprehensive model and experimental validation*, Journal of Crystal Growth 402 (2014) pp. 138-146.

[38] G. del Coso, C. Cañizo, A. Luque, *Radiative energy loss in a polysilicon CVD reactor*, Solar Energy Materials & Solar Cells 95 (2011) pp. 1042-1049.

[39] G. del Coso, *Chemical decomposition of silanes for the production of solar grade silicon*, Ph.D. Thesis, Universidad Politécnica de Madrid - ETSI Telecomunicación, 2010.

[40] A. A. Onischuk, V. N. Panfilov, *Mechanism of thermal decomposition of silanes*, Russian Chemical Reviews 70 (4), (2001) pp. 321-332.

[41] M. P. Bellmann, D. Lindholm, E. A. Sørheim, D. Mortensen, M. M'Hamdi, *3D dynamic simulation of heat transfer and melt flow in a Bridgman growth furnace for mc-silicon with PID temperature control*, Journal of Crystal Growth, Vol. 383 (2013) pp. 119-125.

[42] D. Mortensen, D. Lindholm, K. Friestad, B. R. Henriksen, H. G. Fjær, M. Rudshaug, E. A. Sørheim, *Crystallization furnace modeling including coupled heat and fluid flow, stresses and deformations*, Energy Procedia, Vol. 38 (2013) pp. 597-603.

[43] M. P. Bellmann, D. Lindholm, M. M'Hamdi, *A Novel Method for Gas Flow and Impurity Control in Directional Solidification of Multi-Crystalline Silicon*, Journal of Crystal Growth, Vol. 399 (2014) pp. 33-38.

[44] M. F. Modest, *Radiative Heat Transfer*, Academic Press, New York, 2013.

[45] P. A. Ramachandran, *Advanced Transport Phenomena: Analysis, Modeling and Computing*, Cambridge University Press, 2014.

[46] M. Cohen, D.P. Greenberg, *The hemi-cube: a radiosity solution for complex environments*, In Computer Graphics (Proceedings of SIGGRAPH 85), Vol. 19 (1985) pp. 31-40.

[47] A. Ramos, C. del Cañizo, J. Valdehita, J. C. Zamorano, A. Rodríguez, A. Luque, *Exploring polysilicon deposition conditions through a laboratory CVD prototype*, Physica Status Solidi C 9, No. 10-11 (2012) 2164-2168.

[48] A. Ramos, C. del Cañizo, J. Valdehita, J. C. Zamorano, A. Rodríguez, A. Luque, *On track for Solar Grade Silicon through a Siemens process-type laboratory reactor: operating conditions and energy savings*, Silicon for the Chemical and Solar Industry XI Conference, Norway, 2012.

[49] H. Habuka, Y. Aoyama, S. Akiyama, T. Otsuka, W. F. Qu, M. Shimada, K. Okuyama, *Chemical process of silicon epitaxial growth in a $SiHCl_3$-H_2 system*, Journal of Crystal Growth 207 (1999) pp. 77-86.

[50] W. O. Filtvedt, T. Mongstad, A. Holt, M. Melaaen, H, Klette, *Production of Silicon from SiH4 in a Fluidized Bed, Operation and Results*, International Journal of Chemical Reactor Engineering 11(1), (2013) pp. 1-12.

[51] W. O. Filtvedt, M. Melaaen, A. Holt, M. Javidi, B. R. Olaisen, *Composite Distribution Solution for Minimizing Heat Loss in a Pyrolysis Reactor*, International Journal of Chemical Reactor Engineering, Vol. 9, 2011.

[52] A. A. Istratov, T. Buonassisi, R. J. McDonald, A. R. Smith, R. Schindler, J. A. Rand, J. P. Kalejs, E. R. Weber, *Control of metal impurities in 'dirty' multi-crystalline silicon for solar cells*, Journal of Applied Physics 94 (2003) pp. 6552.

[53] G. Coletti, *Sensitivity of state-of-the-art and high efficiency crystalline silicon solar cells to metal impurities*, Progress in Photovoltaics: Res. Appl. 21 (2013) pp. 1163-1170.

[54] T. Tiedje, E. Yablonovitch, G. D. Cody, B. G. Brooks, *Limiting Efficiency of Silicon Solar Cells*, IEEE Transactions on electronic devices, Vol. 31, no. 5, 1984.

[55] L. C. Rogers, *Polysilicon preparation*, in: W. C. O'Mara (Ed.), Handbook of Semiconductor silicon technology, Noyes Publications, 1990, pp. 33-93.

[56] E. W. Hansen, A. Kjekshus, J. O. Odden, *On the hydrogen in hydrogen-containing amorphous silicon*. Journal of Non-Crystalline Solids 353 (2007) pp. 2734-2743.

[57] J. O. Odden, P. K. Egeberg, A. Kjekshus, *From monosilane to crystalline silicon. Part III. Characterization of amorphous, hydrogen-containing silicon products*, Journal of Non-Crystalline Solids 351 (2005) pp. 1317-1327.

[58] D. Weidhaus, E. Schindlbeck, K. Hesse, E. Dornberger, *Pilot production of granular polysilicon from trichlorosilane using a fluidezed bed-type reactor*, 20th European Photovoltaic Solar Energy Conference, 2005, Spain.